Journal of Power Sources xxx (2009) xxx–xxx

Contents lists available at ScienceDirect

Journal of Power Sources

journal homepage: www.elsevier.com/locate/jpowsour

Structural and electrochemical study of the reaction of lithium with silicon nanowires

Candace K. Chan[a], Riccardo Ruffo[b], Seung Sae Hong[c], Robert A. Huggins[d], Yi Cui[d,*]

[a] Department of Chemistry, Stanford University, Stanford, CA, USA
[b] Department of Materials Science, University of Milan-Bicocca, Milan, Italy
[c] Department of Applied Physics, Stanford University, Stanford, CA, USA
[d] Department of Materials Science and Engineering, Stanford University, Stanford, CA 94305, USA

ARTICLE INFO

Article history:
Received 24 June 2008
Received in revised form 11 December 2008
Accepted 11 December 2008
Available online xxx

Keywords:
Lithium-ion battery
Silicon nanowire
Anode
Phase transformation

ABSTRACT

The structural transformations of silicon nanowires when cycled against lithium were evaluated using electrochemical potential spectroscopy and galvanostatic cycling. During the charge, the nanowires alloy with lithium to form an amorphous Li_xSi compound. At potentials <50 mV, a structural transformation occurs. In studies on micron-sized particles previously reported in the literature, this transformation is a crystallization to a metastable $Li_{15}Si_4$ phase. X-ray diffraction measurements on the Si nanowires, however, show that they are amorphous, suggesting that a different amorphous phase (Li_ySi) is formed. Lithium is removed from this phase in the discharge to form amorphous silicon. We have found that limiting the voltage in the charge to 70 mV results in improved efficiency and cyclability compared to charging to 10 mV. This improvement is due to the suppression of the transformation at low potentials, which alloys for reversible cycling of amorphous silicon nanowires.

1. Introduction

Because of the demand for higher specific energy and energy density lithium batteries for portable electronic devices, electric vehicles, and implantable medical devices, silicon has been studied as a replacement for graphite for the negative electrode.

The incorporation of 4.4 lithium atoms per silicon gives a specific discharge capacity of 4200 mAh g^{-1}. The relatively low potential range at which discharge occurs, below 0.5 V [1], is also attractive. Thus there is a great incentive to find a way to utilize this alloy system. Silicon is the second most abundant element on earth and there is already a mature industrial infrastructure in existence, which also makes it attractive when considering commercial applications.

There have been a number of studies on silicon containing materials involving submicrometer pillars [2], micron- [3] and nano-sized particles [4,5], and various composite anodes [6]. An important feature of all of these silicon-based materials is the large inherent change in specific volume (up to about 400%) during the insertion and extraction of large amounts of silicon [7]. This causes decrepitation, also known as pulverization or crumbling, and a loss of electrical contact between the active material and the current collector. The result is a reduction in the effective capacity during cycling.

In an attempt to better accommodate the large volume change and to avoid capacity loss during cycling due to disconnected material, we have developed an electrode platform that uses nanowires (NWs) vertically adhered to the current collector [8,9]. By exploiting the nanometer size in the diameter while maintaining good electrical contact along the length of the nanowires, we aim to allow for facile volume expansion while preventing decrepitation.

In our previous work [8], we have shown that silicon nanowires (SiNWs) grown directly onto stainless steel current collectors display stable discharge capacities >3000 mAh g^{-1}. Using ex situ scanning electron microscopy (SEM), transmission electron microscopy (TEM), and X-ray diffraction, we observed that the SiNWs remain intact during cycling and become amorphous upon alloying with Li. In this study we used electrochemical potential spectroscopy and galvanostatic cycling to better understand the structural transformations occurring in the SiNWs and how they might affect the reversible cycling.

2. Experimental

2.1. Synthesis

As described previously [8], stainless steel (SS) 304 (0.002 in. thick, McMaster-Carr) substrates were decorated with Au catalyst

* Corresponding author. Tel.: +1 650 723 4613; fax: +1 650 725 4034.
E-mail address: yicui@stanford.edu (Y. Cui).

0378-7753/$ – see front matter © 2008 Elsevier B.V. All rights reserved.
doi:10.1016/j.jpowsour.2008.12.047

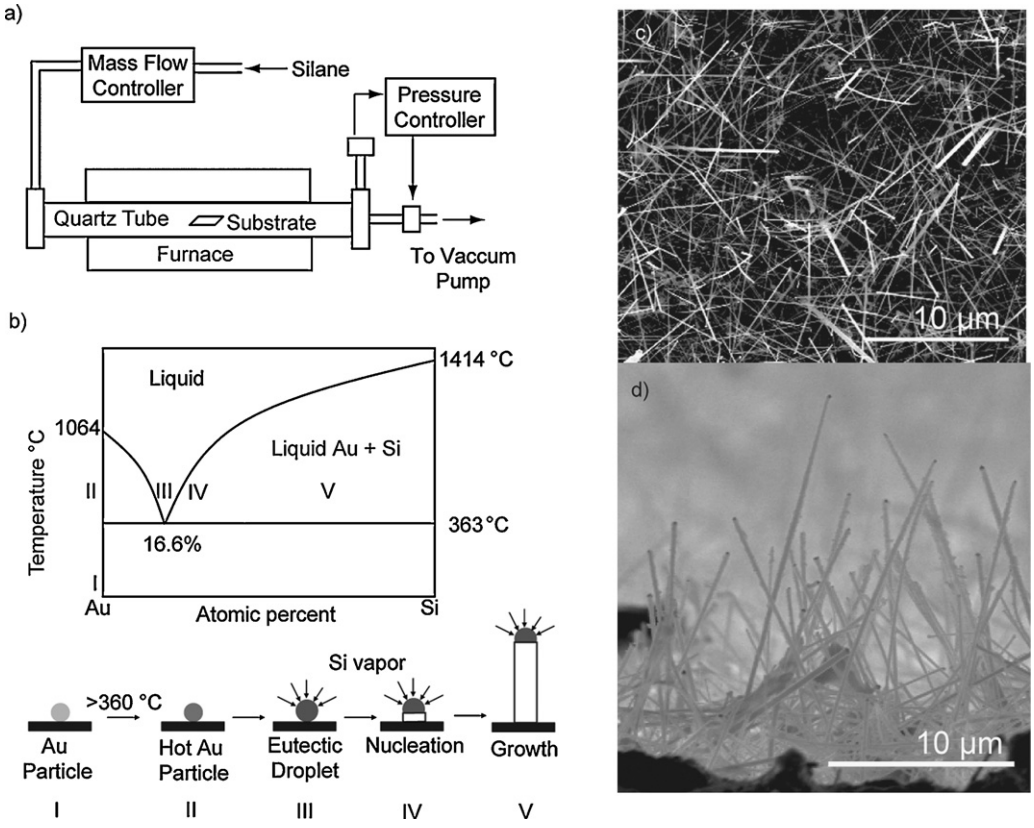

Fig. 1. (a) Apparatus for synthesizing SiNWs. (b) SiNW growth process and corresponding regions on the Si–Au binary phase diagram. (c) SEM image of SiNWs. (d) Side-view SEM image of SiNWs.

by evaporating 50 nm Au using e-beam evaporation and annealing for 30 min at 485 °C just prior to growth. The substrates were heated to 485 °C and silane (SiH_4, 2% in Ar) was flowed in at 50 sccm with a total chamber pressure of 40 Torr for 20 min. The mass of the SiNWs in a given experiment (~200 μg cm^{-2}) was accurately determined by measuring the mass of the substrate using a microbalance (Sartarious SE2, 0.1 μg resolution) before and after growth.

2.2. Electrochemical analysis

Half-cells were fabricated out of the SiNW/SS electrode, Li metal foil, and Celgard 3401 separator soaked in electrolyte. The electrolyte was 1.0 M $LiPF_6$ in 1:1 (w/w) ethylene carbonate:diethyl carbonate (Ferro Corporation). No binders or conducting carbon were used. The cells were assembled inside an Ar-filled glovebox and sealed in aluminized polyethylene laminate bags. The SiNWs were stepped between the open circuit voltage (around 2.5 V) and the lower cutoff voltage (0.01 V) using 5 mV steps. The current was measured in each step until the value was higher than the threshold corresponding to the current of the C/20 charge rate. Each current step was then integrated to get the differential capacity. Galvanostatic measurements were made using a Maccor 4300.

2.3. X-ray diffraction

X-ray diffraction (XRD) was done using a PANalytical X'Pert diffractometer with Cu Kα-radiation. The samples were mounted on the sample stage (DHS900, Anton-Paar) using an Ar-filled transfer bag to prevent exposure to air. The sample stage was covered with a dome made of poly-ether-ether-ketone (PEEK) and filled with Ar to prevent exposure to air during the measurement.

3. Results and discussion

3.1. SiNW growth

The SiNWs were grown directly onto stainless steel substrates as described before [8] inside a tube furnace (Fig. 1a) using the vapor–liquid–solid (VLS) growth method (Fig. 1b). VLS [10,11] is a well-known process for growing NWs that exploits the eutectic region in a binary phase diagram. One of the elements functions as a catalyst for nucleating a NW while the other element is supplied in a vapor form and makes up the bulk of the NW. After the growth, each NW has a catalyst on its tip. For Si, a common catalyst is Au. The Au catalyst is heated (II in Fig. 1b) above the eutectic temperature (363 °C) and SiH_4 is introduced and allowed to decompose into Si. The Si dissolves in the Au particle and forms a eutectic droplet (III in Fig. 1b). Upon reaching supersaturation (IV in Fig. 1b), nucleation of a single-crystalline SiNW occurs. Continuous supply of Si vapor results in increasing growth along the length of the NW (V in Fig. 1b).

Typical SEM images are shown in Fig. 1c and d. The SiNWs had an average diameter of about 100 nm and lengths up to several tens of microns. The cross-section SEM image (Fig. 1d) showed that the SiNWs grew vertically off of the substrate.

3.2. Electrochemical potential spectroscopy

Electrochemical potential spectroscopy [12] was performed to study the differential capacity as a function of potential in the SiNWs and to obtain information about the structural transformations during lithiation and delithiation. The dC/dV vs. voltage and corresponding voltage vs. capacity curves are shown in Fig. 2. Fig. 2a and b shows the curves for charging (lithiation) to 10 mV

Please cite this article in press as: C.K. Chan, et al., J. Power Sources (2009), doi:10.1016/j.jpowsour.2008.12.047

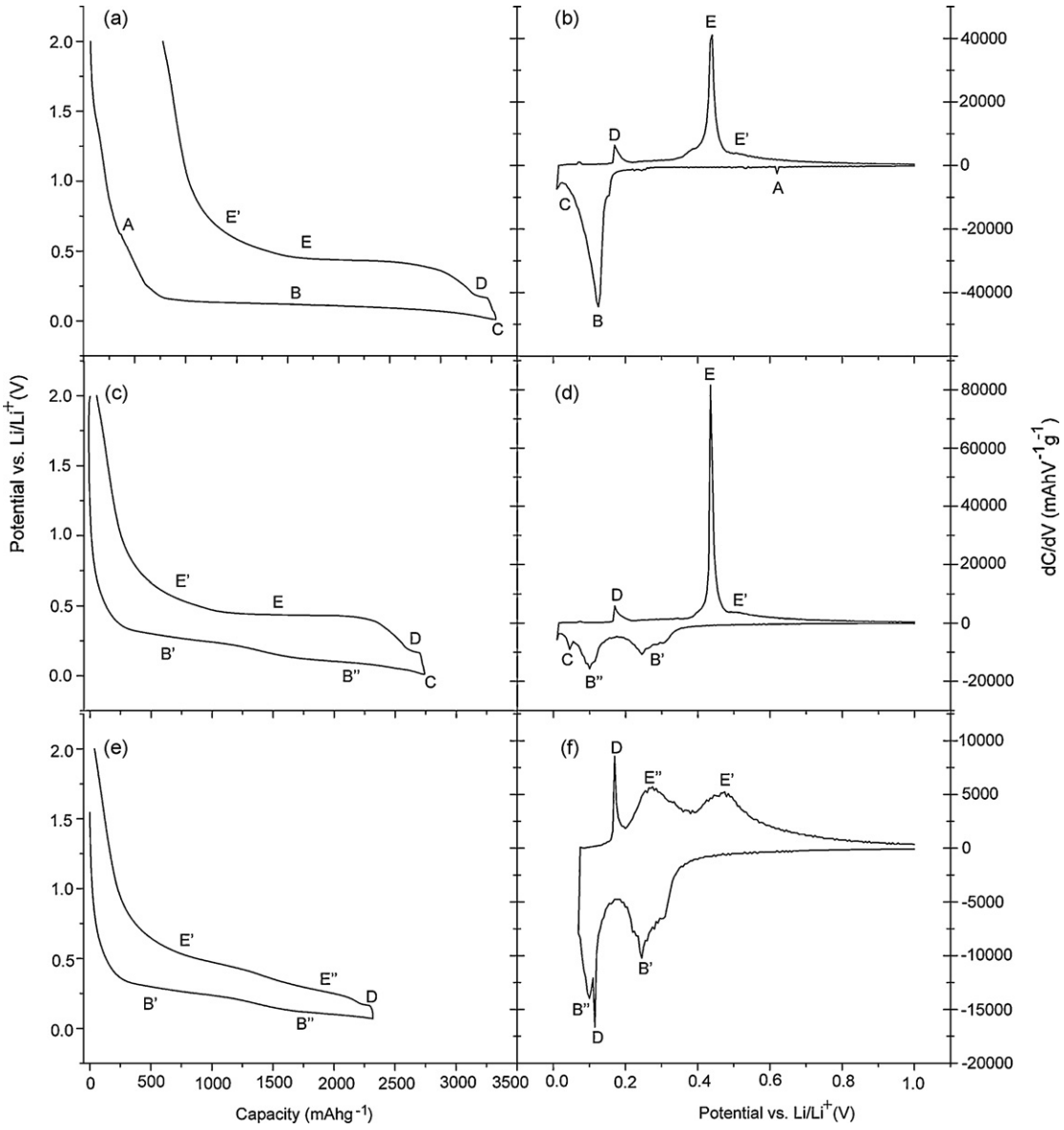

Fig. 2. Electrochemical potential spectroscopy data. Voltage profile (a) and differential capacity curve (b) of the first cycle, starting from crystalline SiNWs and charging to 10 mV. After the first cycle, the SiNWs turned amorphous, resulting in a different voltage profile (c) and differential capacity curve (d). Stopping the charge at 70 mV results in yet another different voltage profile (e) and differential capacity curve (f).

vs. Li/Li^+ and discharging (delithiation) to 2 V vs. Li/Li^+. During the charge, a small peak is observed at 0.62 V and a larger peak at 0.125 V (A and B in Fig. 2b, respectively). The peak at 0.62 V has been reported to be due to SEI formation on the Si surface [5] whereas the peak at 0.125 V is a two-phase region where crystalline Si (c-Si) reacts with Li to form an amorphous lithium silicide, a-Li_xSi [13]. This two-phase region is seen as a long sloping plateau indicated by B in Fig. 2a. The corresponding plateau for the SEI formation in the voltage profile (A in Fig. 2a) is quite small, indicating that this process does not contribute to significant irreversible capacity loss. Indeed, from the peak areas in the differential capacity curve, the capacity due to the SEI peak at 0.62 V was determined to be 253 mAh g^{-1} whereas the capacity due to lithiation of the SiNWs was 2962 mAh g^{-1}. The capacity loss between the charge and discharge was 18%. Because the SEI peak only contributed about 8% of the capacity loss, the cause of the remaining 10% may be due to other factors. Our previous ex situ SEM and TEM work [8] found that the SiNWs did not appear to pulverize or lose contact with the substrate. The cause of the remaining capacity loss is still under investigation.

It has been reported [14] that charging Si to <50 mV results in the formation of a crystalline $Li_{15}Si_4$ phase, which is not predicted by the equilibrium phase diagram. This can be observed as a small peak in the differential capacity curve <50 mV. During discharging, Li is removed from this crystalline phase to form amorphous Si (a-Si) in a two-phase region. This can be observed as a plateau in the voltage profile and a peak in the differential capacity curve. Previously [8], our ex situ XRD and SEM studies failed to observe this crystalline $Li_{15}Si_4$ phase and instead, we only observed that the SiNWs were amorphous. The electrochemical potential spectroscopy data here, however, clearly show a transformation that leads to a two-phase region. During the discharging, two peaks (D and E) are observed in the differential capacity curve (Fig. 2b), which correspond to plateaus in Fig. 2a. The two-phase region at E looks similar to the reported [13] delithiation of crystalline $Li_{15}Si_4$ to form amorphous Si. However, our XRD data do not support the formation of the crystalline $Li_{15}Si_4$ phase. XRD scans taken of samples charged

Please cite this article in press as: C.K. Chan, et al., J. Power Sources (2009), doi:10.1016/j.jpowsour.2008.12.047

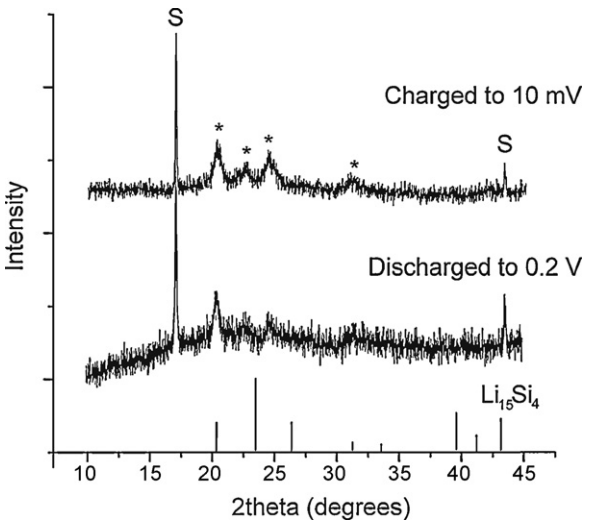

Fig. 3. X-ray diffraction data of SiNWs charged to 10 mV and discharged to 2.0 V. The peaks marked by S are from the stainless steel substrate. The peaks marked with * are from the PEEK dome on the sample stage. The $Li_{15}Si_4$ peaks, which are overlaid as a reference, do not appear in the scans.

to 10 mV and discharged to 0.2 V clearly showed the absence of any crystalline phase (Fig. 3). Based on our EPS data, if the crystalline $Li_{15}Si_4$ phase had formed, it should exist at both of these potentials. The absence of the phase in the XRD data suggests that the SiNWs remain amorphous. Although the EPS data look very similar to that reported in the literature, we do not believe the feature at C and E are due to crystalline $Li_{15}Si_4$ formation and delithiation, respectively. Instead, it is possible that the transformation at C is the formation of a distinct amorphous lithium silicide phase, here called a-Li_ySi, which is different from the a-Li_xSi formed during the charge (region B). The feature at E then may be a two-phase region between two different amorphous lithiated phases.

Fig. 2c and d shows the voltage and dC/dV curves after the crystalline Si has been converted to amorphous Si following the first cycle. During the charge, lithiation into the amorphous Si occurs in two sloping single-phase regions, as indicated by B′ and B″. The lithiation of amorphous Si in two different voltage regions has been reported previously [13], but the reason for it is still unknown and requires further investigation. Here, we use a-$Li_{x'}Si$ to identify the phase formed at B′, and a-$Li_{(x'+x'')}Si$ to identify the phase formed at B″. Below 50 mV, the same transformation to a-Li_ySi occurs and delithiation of this phase occurs in a two-phase region to show a similar plateau as in Fig. 2a.

Limiting the voltage of the charge to >70 mV prevents the formation of the a-Li_ySi phase, as shown in Fig. 2e and f. Delithiation thus occurs in two single-phase regions, as indicated by E′ and E″. At E′, the a-$Li_{x'}Si$ phase is delithiated to a-Si. The voltage profile (Fig. 2e) is thus characterized by sloping regions due to cycling of amorphous Si rather than a plateau as seen in Fig. 2a and d. Closer inspection of the voltage profiles indicate that the delithiation noted by E′ is observed even after charging to <70 mV, as indicated in Fig. 2a and c. In the dC/dV curve, this feature is observed after the large peak at E. Thus, we conclude that during the process at E, there is a two-phase region between a-Li_ySi and a-$Li_{x'}Si$. Then at E′, the a-$Li_{x'}Si$ is delithiated to a-Si.

The features indicated by D were due to alloying of the Au catalyst with the Li. Au has been known to react with Li at low potentials [15]. Control experiments of a 50-nm film of Au showed that a charge capacity of 47 mAh g^{-1} could be obtained due to lithiation of Li with Au as determined using electrochemical potential spectroscopy with a C/20 cutoff current. This corresponds to a stoichiometry of $Li_{0.331}Au$. However, galvanostatic cycling

Table 1
Summary of phase transformations in SiNWs.

Point in Fig. 2	Reaction
A	SEI formation
B	Lithiation of crystalline Si, c-Si + xLi → a-Li_xSi
C	Transformation to new phase at <50 mV, a-Li_xSi → a-Li_ySi
D	Gold alloying/dealloying with Li
E	Delithiation of phase formed at <50 mV a-Li_ySi → a-$Li_{x'}Si$ + $(y - x')$Li
B′	Lithiation of amorphous Si at >0.17 V, a-Si + x'Li → a-$Li_{x'}Si$
B″	Lithiation of amorphous Si between 70 mV and 0.17 V a-$Li_{x'}Si$ + x''Li → a-$Li_{(x'+x'')}Si$
E″	Delithiation of amorphous Si <0.38 V a-$Li_{(x'+x'')}Si$ → a-$Li_{x'}Si$ + x''Li
E′	Delithiation of amorphous Si >0.38 V, a-$Li_{x'}Si$ → a-Si + x'Li

using a C/5 rate showed lower capacities (20–35 mAh g^{-1}) that quickly degraded with each cycle, suggesting that the process is not reversible over many cycles and may also be kinetically limited. The "trapping" of Li into the Au may be one possible reason for the capacity loss we have observed in the SiNW samples, and this is still under investigation.

Based on the electrochemical potential data (summarized in Table 1), we found that the SiNWs appear to undergo similar phase transformations as observed in previous studies in micron-sized crystalline Si powders [13,16]. However, XRD data suggest that the structural transformations at low potentials are different in the SiNWs. Because our SiNWs have a cylindrical geometry and space to freely expand, formation of the $Li_{15}Si_4$ phase may be dependent on parameters other than the voltage of the charge, such as strain with the substrate and/or film thickness. Indeed, previous studies done on amorphous Si thin films [17] observed that formation of $Li_{15}Si_4$ did not occur for films with thicknesses <2.5 μm.

3.3. Galvanostatic cycling

Different galvanostatic charge/discharge measurements were made to determine how the structural changes affected the reversible cyclability. Fig. 4a shows cycling done using a C/20 rate between 10 mV and 2.0 V. In the voltage profile, the plateau characteristic of lithiation of crystalline Si is observed in the first charge. Afterwards, the charges have the sloping profiles characteristic of lithiation of amorphous Si in two different voltage regions. All of the discharges show plateaus due to delithiation of the a-Li_ySi phase. Fig. 4b shows cycling done using a C/5 rate using the same voltage range. Interestingly, all of the discharges show sloping profiles, although there is still an indication of a plateau, suggesting partial formation of a-Li_ySi. This suggests that formation of the a-Li_ySi phase may be rate dependent or that there may be polarization in the electrode. The C/5 cycling also showed improved coulombic efficiency and lower irreversible capacity loss in the first cycle. The reason for this improvement in cycling may be due to several reasons. The first may be due to increased side reactions with the electrolyte or more Li–Au alloy formation at the lower rate. The second may be due to improved cycling due to the suppression of the formation of the a-Li_ySi phase. Highly reversible cycling of amorphous Si thin films has been reported [18], with the good cyclability being attributed to the facile Li insertion and extraction into the single phase.

In order to better understand this improved cyclability at the C/5 rate, we performed galvanostatic measurements with different voltage cutoffs in the charge to control the formation of the a-Li_ySi phase. Fig. 4c shows the cycling profile of a sample cycled between 70 mV and 2.0 V. Compared to Fig. 4b (10 mV cutoff, C/5 rate), the discharge curves clearly show amorphous cycling. The first charge

Please cite this article in press as: C.K. Chan, et al., J. Power Sources (2009), doi:10.1016/j.jpowsour.2008.12.047

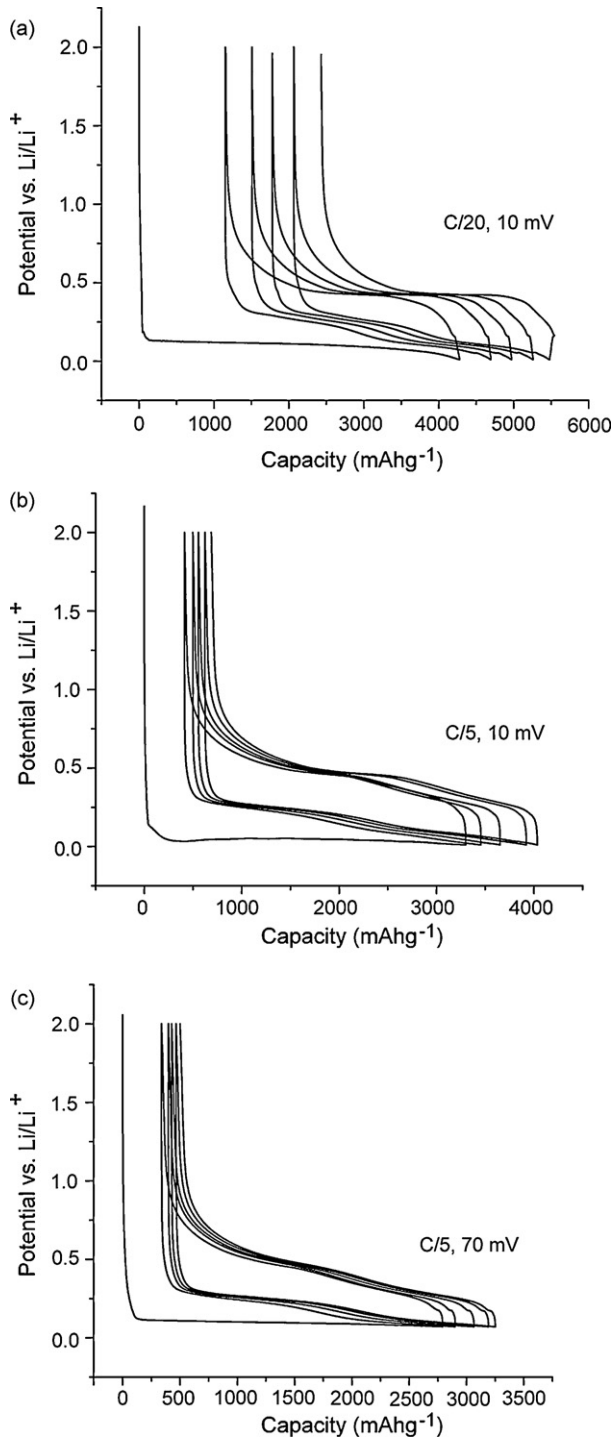

Fig. 4. Galvanostatic cycling of SiNWs at (a) C/20 rate with charge to 10 mV, (b) C/5 rate with charge to 10 mV and (c) C/5 rate with charge to 70 mV.

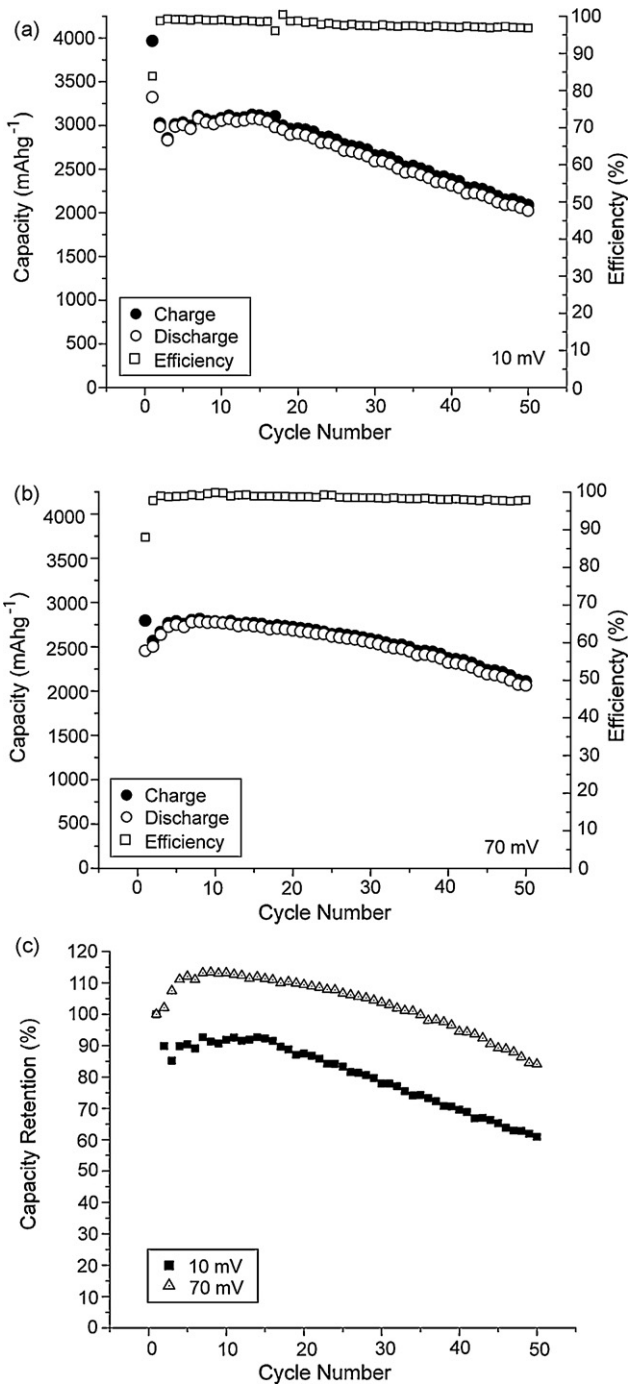

Fig. 5. Cycle life of SiNWs cycled at (a) C/5 rate with charge to 10 mV, (b) C/5 rate with charge to 70 mV and (c) the discharge capacity retention for the samples charged to 10 mV compared to 70 mV.

capacity for the 70 mV cutoff is lower than for the 10 mV cutoff, as expected, due to fewer Li ions being inserted. However, the cycling with the 70 mV cutoff has better reversibility than the 10 mV cutoff. This may be due to improved reversibility when cycling only amorphous Si.

3.4. Cycle life

The cycle life of the SiNWs measured with different charge cutoffs was monitored for 50 cycles (Fig. 5). For the 10 mV cutoff (Fig. 5a), both charge and discharge capacities were quite stable, with a coulombic efficiency of 99% (84% in the first cycle), for about 16 cycles, after which the capacity began to drop. After 50 cycles, the capacity retention was 61% (Fig. 5c). For the 70 mV cutoff, the results are quite different (Fig. 5b). The irreversible capacity loss in the first cycle is lower (12%) than for the 10 mV (16%) case. Also, the capacity retention after 50 cycles is much higher. This suggests that suppression of the crystallization of a-Li_ySi may substantially improve the reversible cycling of the SiNWs.

Please cite this article in press as: C.K. Chan, et al., J. Power Sources (2009), doi:10.1016/j.jpowsour.2008.12.047

4. Conclusions

Here we report the structural transformations occurring in the SiNWs when cycled with Li. In contrast to studies reported on Si powders, the SiNWs do not appear to recrystallize at low potentials, although a transformation event to a different phase may be occurring. Because XRD data do not indicate a crystalline phase, we conclude that this phase is an amorphous lithium silicide. In our potential spectroscopy analysis, we therefore observe four different amorphous lithium silicides: during the lithiation of crystalline Si in the first charge (a-Li_xSi), at potentials <50 mV (a-Li_ySi), and during lithiation of amorphous Si in all subsequent charges (a-$Li_{x'}Si$ and a-$Li_{(x'+x'')}Si$). From our galvanostatic studies at different rates and using different voltage cutoffs in the charge, it is clear that these amorphous phases can contribute to the reversibility and cycling retention. There is also indication that formation of these phases, particularly the a-Li_ySi phase, is kinetically limited. Therefore, although characterization of these amorphous phases may be challenging, understanding them may be key to developing better silicon-based negative electrodes for lithium batteries.

Acknowledgments

C.K.C. acknowledges support from a National Science Foundation graduate fellowship and Stanford Graduate Fellowship. Y.C. acknowledges support from the Global Climate and Energy Project at Stanford, US Office of Naval Research and King Abdullah University of Science and Technology.

References

[1] C.J. Wen, R.A. Huggins, J. Solid State Chem. 37 (1981) 271.
[2] M. Green, E. Fielder, B. Scrosati, M. Wachtler, J.S. Moreno, Electrochem. Solid-State Lett. 6 (2003) A75–A79.
[3] J.H. Ryu, J.W. Kim, Y.-E. Sung, S.M. Oh, Electrochem. Solid-State Lett. 7 (2004) A306–A309.
[4] H. Li, X. Huang, L. Chen, Z. Wu, Y. Liang, Electrochem. Solid-State Lett. 2 (1999) 547–549.
[5] J. Graetz, C.C. Ahn, R. Yazami, B. Fultz, Electrochem. Solid-State Lett. 6 (2003) A194–A197.
[6] U. Kasavajjula, C. Wang, A.J. Appleby, J. Power Sources 163 (2007) 1003–1039.
[7] B.A. Boukamp, G.C. Lesh, R.A. Huggins, J. Electrochem. Soc. 128 (1981) 725–729.
[8] C.K. Chan, H. Peng, G. Liu, K. McIlwrath, X.F. Zhang, Y. Cui, Nat. Nanotechnol. 3 (2008) 31–35.
[9] C.K. Chan, X.F. Zhang, Y. Cui, Nano Lett. 8 (2008) 307–309.
[10] R.S. Wagner, W.C. Ellis, Appl. Phys. Lett. 4 (1964) 89.
[11] A.M. Morales, C.M. Lieber, Science 279 (1998) 208–211.
[12] A.H. Thompson, J. Electrochem. Soc. 126 (1979) 608–616.
[13] M.N. Obrovac, L.J. Krause, J. Electrochem. Soc. 154 (2007) A103–A108.
[14] M.N. Obrovac, L. Christensen, Electrochem. Solid-State Lett. 7 (2004) A93–A96.
[15] G. Taillades, N. Benjelloun, J. Sarradin, M. Ribes, Solid State Ionics 152–153 (2002) 119–124.
[16] J. Li, J.R. Dahn, J. Electrochem. Soc. 154 (2007) A156–A161.
[17] T.D. Hatchard, J.R. Dahn, J. Electrochem. Soc. 151 (2004) A838–A842.
[18] T. Takamura, S. Ohara, M. Uehara, J. Suzuki, K. Sekine, J. Power Sources 129 (2004) 96–100.